Control Engineering Practice 152 (2024) 106067

Contents lists available at ScienceDirect

Control Engineering Practice

journal homepage: www.elsevier.com/locate/conengprac

Iterative-only learning control for soft landing of short-stroke reluctance actuators

Eduardo Moya-Lasheras *, Carlos Sagues

Departamento de Informatica e Ingenieria de Sistemas (DIIS) and Instituto de Investigacion en Ingenieria de Aragon (I3A), Universidad de Zaragoza, Zaragoza, 50018, Spain

ARTICLE INFO

Keywords:
Electromechanical devices
Iterative learning control
Relays
Soft landing
Switches
Valves

ABSTRACT

Short-stroke reluctance actuators, such as electromechanical relays and solenoid valves, often experience strong impacts at the end of standard switching operations, leading to problems like contact bounces, mechanical wear or acoustic noise. This paper introduces a novel iterative learning controller for tracking the actuator position during switching operations and ultimately decreasing the impact velocities. The control strategy is designed based on a generalized dynamical description, allowing for its application to a broad range of actuators and models. A highlight of the proposal is the absence of a real-time feedback controller, which eliminates the need for real-time measurements. Another important feature is the adaptation of the learning control gain based on a soft-landing performance index. The control performance is analyzed and validated in conjunction with an offline position estimator through Monte Carlo simulations and experimental testing. The results show that the position tracking remains accurate even in the presence of non-repeating perturbations and estimation errors, leading to a substantial reduction in switching impacts.

1. Introduction

Reluctance actuators are electromagnetic devices that rely on reluctance-based magnetic forces between ferromagnetic movers and stators. Compared with voice coil actuators, they can produce larger forces with less moving mass and power dissipation (Vrijsen et al., 2010). Thus, there is an increasing interest in incorporating these devices in many applications, e.g., fast tool servos for diamond turning (Lu & Trumper, 2005), propulsion systems for elevators (Lim et al., 2008), beam pointing and stabilization in optical systems (Kluk et al., 2012), anti-vibration systems (Bao et al., 2014), linear compressors (Xue et al., 2018), or flexure-guided nanopositioning (Ito et al., 2019).

More specifically, the devices under study in this paper are short-stroke (switch-type) reluctance actuators, characterized by their constrained motion. They are mostly used for opening and closing electrical, pneumatic or hydraulic circuits. For example, electromechanical relays (Fig. 1) are utilized for power switching operations, while solenoid valves (Fig. 2) are used for fluid flow regulation. A well-known problem of the switching actuation is the strong landing impacts that cause mechanical wear, bouncing and acoustic noise. These decrease the reliability of the actuators and narrow the range of suitable applications. Thus, there is a great interest in the research of soft-landing controllers to reduce the impact velocities at the end of switching operations.

There is extensive literature that deals with the soft-landing control of reluctance actuators, although the majority of them focus on more complex and expensive devices (e.g. with permanent magnets, multiple coils and springs, or position sensors). The most conventional and common approach is to track a desired position trajectory. Many types of feedback controllers (FBC) have been proposed for position tracking, such as linear–quadratic (Hoffmann et al., 2003; Tai & Tsao, 2003), backstepping (Benosman & Atinç, 2015; Kahveci & Kolmanovsky, 2010), sliding-mode (Di Bernardo et al., 2012; Moya-Lasheras et al., 2020a), or flatness-based (Chladny & Koch, 2008; Gill et al., 2015). Given the repetitive nature of the switching operations, some authors propose run-to-run learning-type controllers to adjust the feedback or feedforward controller while optimizing an auxiliary variable related to each commutation performance, e.g., final tracking error (Benosman & Atinç, 2015; Mercorelli, 2012), impact velocity (Di Gaeta et al., 2015; Yang et al., 2013), acoustic noise (Moya-Lasheras & Sagues, 2020; Peterson & Stefanopoulou, 2004), or bouncing duration (Ramirez-Laboreo et al., 2017). An alternative approach for cycle-to-cycle adaptation is iterative learning control (ILC), which is more effective than run-to-run strategies at controlling processes with frequent measurements of the tracked variable (Wang et al., 2009). This learning-type strategy has already been proposed for a different type of

* Corresponding author.
E-mail address: emoya@unizar.es (E. Moya-Lasheras).

https://doi.org/10.1016/j.conengprac.2024.106067
Received 16 October 2023; Received in revised form 22 August 2024; Accepted 23 August 2024
Available online 2 September 2024

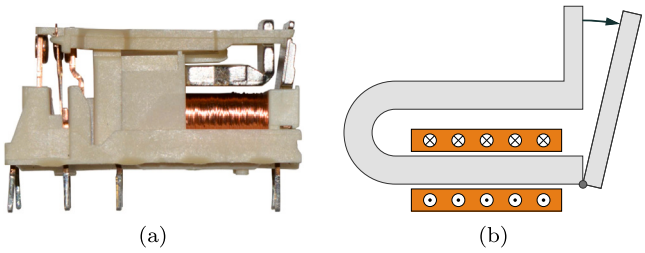

Fig. 1. Electromechanical relay. (a) Photo. (b) Schematic diagram.

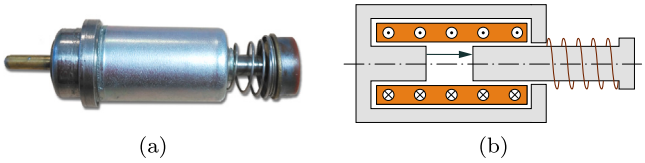

Fig. 2. Solenoid valve. (a) Photo. (b) Schematic diagram.

reluctance actuators, specifically double-coil and double-spring valves for camless engines (Hoffmann et al., 2003; Tai & Tsao, 2003).

One important drawback of FBC and ILC tracking controllers is their need of position measurements or estimates within the switching intervals. The utilization of position sensors, while ideal, proves unfeasible or cost-prohibitive in numerous scenarios, particularly for small, fast, and economical actuators. The cost of accurate and sufficiently rapid sensors can be several orders of magnitude higher than that of the devices themselves. An alternative is position estimation from other measurable variables, such as coil voltage and current. Different types of observers have been proposed for reluctance actuators, such as extended Kalman filters (Pedersen et al., 2022), unscented Kalman filters (Moya-Lasheras et al., 2017), sliding-mode observers (Braun et al., 2019), or open-loop techniques with no output-based correction (Katalenic et al., 2016). However, these approaches are impractical in many applications, because the dynamics are very complex (models are highly nonlinear) and fast (commutations typically last few milliseconds). Furthermore, they are quite sensitive to modeling errors, which is very difficult to overcome when there is a high variability between units and fine-tuning the model parameters for every device is not feasible.

An unexplored third approach is the offline estimation of position trajectories, which is easier to implement than its real-time counterpart and, most importantly, it is more accurate (Moya-Lasheras et al., 2022). ILC solutions can use offline estimators, but previous ILC implementations (Hoffmann et al., 2003; Tai & Tsao, 2003) also rely on FBC and thus on online position sensing or estimation. Note also that run-to-run controllers may also be designed for taking advantage of offline position estimators, but previous approaches have been implemented and tested with simulated position (Moya-Lasheras & Sagues, 2020) or measured position (Yang et al., 2013). There are ILC proposals for various applications without real-time FBC (some recent examples are Sa-e et al. (2020), Upadhyay and Schaal (2020) and Ketelhut et al. (2019)). However, to the best of the authors' knowledge, it has not yet been successfully designed and implemented for the studied class of actuators.

In general, for highly nonlinear and uncertain systems, simple first-order linear ILC laws, also known as proportional-type ILC, are remarkably effective (Xu, 2011). Moreover, to better deal with uncertainties, adaptation laws can be incorporated. Most adaptation proposals are based on conventional adaptation laws for real-time feedback controllers, modifying model parameter estimates that are used in the ILC control law (Chien & Tayebi, 2008; Huang et al., 2021; Li et al., 2019). However, there are other methods for adapting the control

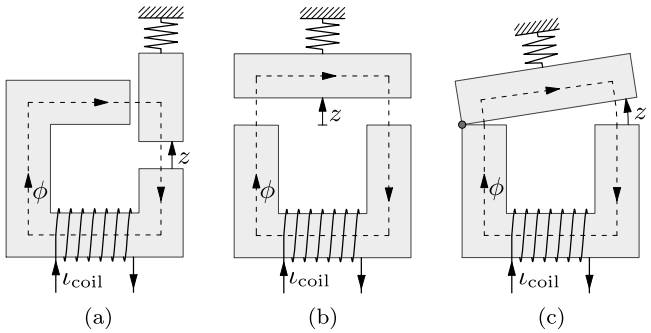

Fig. 3. Schematic representation of single-coil reluctance actuators.

law, focusing on improving robustness or performance, such as time-varying Q-filter (Bristow & Alleyne, 2008; Rotariu et al., 2008), time-varying control gain (Moore et al., 2005), or iteration-varying control gain (Owens & Munde, 1998).

This paper presents the design of an ILC for position tracking and soft landing of short-stroke reluctance actuators. The approach is based on a generalized dynamical description of reluctance actuators, derived from the continuous-time version presented in a previous work (Moya-Lasheras et al., 2022). It has been extended to allow for an arbitrary number of core parts, each with different shapes and magnetomotive forces, thus broadening the applicability of the control technique. Additionally, the ILC does not rely on any real-time FBC, making it compatible with offline estimators or sensors. The paper proposes methods to overcome the limitations imposed by the lack of FBC, in particular the novel concept of adapting the ILC gain using a performance index aligned with the ultimate goal of soft landing. An additional contribution is the use of the controller combined with an offline position estimator, which is analyzed through simulation and experimentation. It is also the first validation of this position estimator in the context of control.

2. General dynamical description

The devices under study are simple low-cost actuators, with a single coil and no permanent magnets. For example, Fig. 3 depicts schematic representations of some of these actuators. For each one, the magnetic core is divided into two parts: a fixed part (stator) and a movable part (mover or armature). The air gaps between the core parts depend on the position of the mover z, which is restricted between a lower and an upper limit. The motion may be linear (Figs. 3(a) and 3(b)) or angular (Fig. 3(c)). The electrical current through the coil $\imath_{\text{coil}}$ generates a magnetic flux ϕ through the core parts and the air gaps between them, which results in a magnetic force. There are two asymmetrical operation types: closing and opening, in the direction of the magnetic force or other passive forces, respectively.

We present a generalized dynamical description that serves as the basis of the control design. For clarity, the system is separated into the electromagnetic and mechanical parts.

2.1. Electromagnetic dynamics

The electromagnetic system is governed by two main equations. The first one is the electrical circuit equation of the coil,

$$\upsilon_{\text{coil}} = R\,\imath_{\text{coil}} + N\,\dot{\phi}, \tag{1}$$

where υ_{coil}, R and N are the coil voltage, resistance and number of turns, respectively. The second equation is Ampère's circuital law, which relates the current passing through a surface with the magnetomotive force across the closed boundary curve from said surface. By

defining the curve as the path of the magnetic flux (see each actuator represented in Fig. 3), the derived equation is

$$N\,\imath_{\text{coil}} + \imath_{\text{eddy}} = \mathcal{F}_{\text{c}} + \mathcal{F}_{\text{g}}, \tag{2}$$

where $\imath_{\text{eddy}}$ is the net eddy current through the core, and $\mathcal{F}_{\text{c}}$ and $\mathcal{F}_{\text{g}}$ are the magnetomotive forces of the core and gap.

To characterize the eddy currents, it is assumed that the magnetic flux is uniform within the cross section of the core. This results in the following relation:

$$\imath_{\text{eddy}} = -k_{\text{eddy}}\,\dot{\phi}, \tag{3}$$

where k_{eddy} is a positive constant that depends on the geometry and conductivity of the core (Ramirez-Laboreo, 2019).

Moreover, the gap magnetomotive force can be directly related to the magnetic flux based on the magnetic reluctance definition. Specifically,

$$\mathcal{F}_{\text{g}} = \sum_i \mathcal{R}_{\text{g}_i}(z)\,\phi = \mathcal{R}_{\text{g}}(z)\,\phi, \tag{4}$$

where $\mathcal{R}_{\text{g}_i}$ denotes the magnetic reluctance of each gap, and $\mathcal{R}_{\text{g}}$ the resulting total reluctance. Note that it depends on the gap length that, in turn, depends on the actuator position z (see Fig. 3).

In contrast, the relation between the core magnetomotive force and the magnetic flux presents a hysteretic behavior. Thus, the reluctance approximation can only be applied if the magnetic hysteresis phenomenon is neglected. As a more comprehensive approach, the proposed characterization uses a differential counterpart of the reluctance, which is defined differently for increasing and decreasing magnetic flux. Firstly, the total magnetomotive force is divided into an arbitrary number of terms $\mathcal{F}_i$, corresponding to several core parts which may have different shapes. It can be expressed as follows:

$$\mathcal{F}_{\text{c}} = \sum_i \mathcal{F}_i, \qquad \boldsymbol{\mathcal{F}} = \begin{bmatrix}\mathcal{F}_1 & \mathcal{F}_2 & \cdots\end{bmatrix}^{\mathsf{T}}. \tag{5}$$

Then, a differential reluctance for each core part $\mathcal{R}_{\Delta i}$ is formally defined as a piece-wise function,

$$\mathcal{R}_{\Delta i}(\mathcal{F}_i, \phi, \dot{\phi}) = \frac{\mathrm{d}\mathcal{F}_i}{\mathrm{d}\phi} = \begin{cases} \mathcal{R}^{+}_{\Delta i}(\mathcal{F}_i, \phi), & \text{if } \dot{\phi} \geq 0 \\ \mathcal{R}^{-}_{\Delta i}(\mathcal{F}_i, \phi), & \text{if } \dot{\phi} < 0. \end{cases} \tag{6}$$

This proposed approach is general enough to encompass certain hysteresis models, e.g. Jiles–Atherton (Moya-Lasheras et al., 2021); and non-hysteretic reluctance-based ones, in which case $\mathcal{R}^{+}_{\Delta i} = \mathcal{R}^{-}_{\Delta i}$.

Finally, substituting (3)–(5) into (2), and isolating the magnetic flux derivative, the following differential equation is derived:

$$\dot{\phi} = -\frac{\mathcal{R}_{\text{g}}(z)\,\phi + \sum_i \mathcal{F}_i}{k_{\text{eddy}}} + \frac{N}{k_{\text{eddy}}}\,\imath_{\text{coil}}, \tag{7}$$

where the current $\imath_{\text{coil}}$ would act as the input. However, it is more common to control the actuators with the voltage υ_{coil} as the input. Then, from (1) and (7), the corresponding differential equation is defined as

$$\dot{\phi} = -\frac{R\left(\mathcal{R}_{\text{g}}(z)\,\phi + \sum_i \mathcal{F}_i\right)}{N^2 + R\,k_{\text{eddy}}} + \frac{N}{N^2 + R\,k_{\text{eddy}}}\,\upsilon_{\text{coil}}. \tag{8}$$

Regardless of the chosen input u, the dynamics of the magnetic flux is given by an input-affine nonlinear function,

$$\dot{\phi} = f_{\phi}(z, \phi, \boldsymbol{\mathcal{F}}) + g_{\phi}\,u. \tag{9}$$

Consequently, the dynamics of core magnetomotive force can be represented with a vector function of the same variables,

$$\dot{\boldsymbol{\mathcal{F}}} = \boldsymbol{f}_{\boldsymbol{\mathcal{F}}}(z, \phi, \boldsymbol{\mathcal{F}}, u), \tag{10}$$

where each scalar component is given by (6) and (9),

$$f_{\mathcal{F}_i}(z, \phi, \boldsymbol{\mathcal{F}}, u) = \mathcal{R}_{\Delta i}\left(\mathcal{F}_i, \phi, \dot{\phi}\right)\dot{\phi}, \qquad \dot{\phi} = f_{\phi}(z, \phi, \boldsymbol{\mathcal{F}}) + g_{\phi}\,u. \tag{11}$$

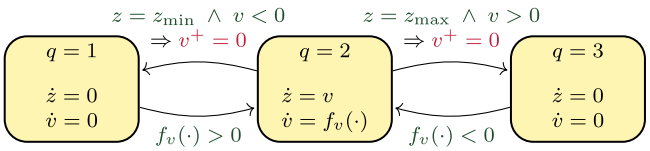

Fig. 4. Diagram of the hybrid automaton describing the mechanical subsystem, including the position constraints. Each transition between modes (yellow blocks) occurs when the corresponding guard condition (green text, before "⇒") is satisfied. In some transitions, the velocity jumps according to the corresponding reset rule (red text, after "⇒"). (For interpretation of the references to color in this figure legend, the reader is referred to the web version of this article.)

2.2. Mechanical dynamics

The dynamical equation of the armature during motion is given by Newton's second law. Following a state-space representation, the position z and velocity v are treated as state variables, whose dynamical equations during motion are

$$\dot{z} = v, \tag{12}$$

$$\dot{v} = f_v(z, v, \phi) = \frac{1}{m}\left(F_{\text{pas}}(z, v) - F_{\text{mag}}(z, \phi)\right), \tag{13}$$

where m is the movable mass, F_{mag} is the magnetic force, and F_{pas} is the passive force that encompasses the remaining forces acting on the mover (e.g., elastic, gravitational or friction forces). The only force that can be controlled — albeit indirectly — is the magnetic force, which is defined (Moya-Lasheras et al., 2021) as

$$F_{\text{mag}}(z, \phi) = -\frac{1}{2}\,\mathcal{R}'_{\text{g}}(z)\,\phi^2, \qquad \mathcal{R}'_{\text{g}}(z) = \frac{\partial \mathcal{R}_{\text{g}}(z)}{\partial z}. \tag{14}$$

Note that the stroke of these actuators is limited. Thus, the mechanical dynamics must change when resting in the minimum position $z_{\min}$ or maximum position $z_{\max}$. This is achieved by representing the dynamics with a hybrid automaton, as depicted in Fig. 4. The dynamic mode is given by the discrete state $q \in \{1, 2, 3\}$. Each transition between two modes is accompanied by its guard condition and, in the case of transitioning from $q = 2$, also a reset function: $v^+ = 0$.

3. Iterative learning control

3.1. Problem formulation

The controller is initially designed based on the dynamical equations of the motion mode ($q = 2$), which can be expressed compactly as

$$\dot{\boldsymbol{x}}_n(t) = \boldsymbol{f}\left(\boldsymbol{x}_n(t), u_n(t)\right), \tag{15a}$$

$$y_n(t) = h\left(\boldsymbol{x}_n(t), u_n(t)\right), \tag{15b}$$

where $\boldsymbol{x}_n$ is the state vector and y_n is the output. Note that n and t denote the iteration and time dependence, respectively. To improve the readability of the following expressions, the iteration and time dependence of variables is omitted whenever possible.

In accordance to the notation from Section 2, the state vector and function are

$$\boldsymbol{x} = \begin{bmatrix} z \\ v \\ \phi \\ \boldsymbol{\mathcal{F}} \end{bmatrix}, \qquad \boldsymbol{f}(\boldsymbol{x}, u) = \begin{bmatrix} v \\ f_v(z, v, \phi) \\ f_{\phi}(z, \phi, \boldsymbol{\mathcal{F}}) + g_{\phi}\,u \\ \boldsymbol{f}_{\boldsymbol{\mathcal{F}}}(z, \phi, \boldsymbol{\mathcal{F}}, u) \end{bmatrix}. \tag{16}$$

On the other hand, the output is specified as the variable to be tracked through control. The objective is to track the position z. However, in order to facilitate the control design and theoretical analysis, the following output is instead proposed:

$$y = h(\boldsymbol{x}, u) = \left(\varrho + \frac{\mathrm{d}}{\mathrm{d}t}\right)^3 z = \varrho^3\,z + 3\,\varrho^2\,v + 3\,\varrho\,a + \dot{a}, \tag{17}$$

being ϱ a positive constant, a the acceleration and $\dot{a}$ the jerk,

$$a = f_v(z, v, \phi), \qquad \dot{a} = \mathrm{d}f_v/\mathrm{d}t. \tag{18}$$

Note that the relation between y and z (17) can be interpreted as a third-order linear time-invariant dynamical system, where $-\varrho$ are the system poles. Thus, the constant ϱ can be specified for a desired settling time. Note also that the jerk can be expressed compactly as an input-affine function,

$$\dot{a} = f_a(\boldsymbol{x}) + g_a(\boldsymbol{x})\, u, \tag{19}$$

where

$$f_a(\boldsymbol{x}) = \frac{\partial f_v}{\partial z}\, v + \frac{\partial f_v}{\partial v}\, f_v(z, v, \phi) + \frac{\partial f_v}{\partial \phi}\, f_\phi(z, \phi, \boldsymbol{\mathcal{F}}), \tag{20}$$

$$g_a(\boldsymbol{x}) = \frac{\partial f_v}{\partial \phi}\, g_\phi, \tag{21}$$

which, in turn, depend on the following partial derivatives:

$$\frac{\partial f_v}{\partial z} = \frac{1}{m}\left(\frac{\partial F_{\mathrm{pas}}}{\partial z}(z, v) - \frac{1}{2}\,\mathcal{R}_{\mathrm{g}}''(z)\,\phi^2\right), \tag{22}$$

$$\frac{\partial f_v}{\partial v} = \frac{1}{m}\,\frac{\partial F_{\mathrm{pas}}}{\partial v}(z, v), \tag{23}$$

$$\frac{\partial f_v}{\partial \phi} = -\frac{1}{m}\,\mathcal{R}_{\mathrm{g}}'(z)\,\phi. \tag{24}$$

Furthermore, for the theoretical design and convergence proof of the controller, it is necessary to establish a set of assumptions. The first two are well known and widely used for ILC design, while the last three are specifically tailored for the studied systems:

Assumption 1. For any input signal and initial state vector, the state vector $\boldsymbol{x}(t)$ and function $\boldsymbol{f}$ (16) are bounded.

Assumption 2. For every iteration n, the initial values of the state vector $\boldsymbol{x}_n(t)$ are identical and equal to the desired ones $\boldsymbol{x}_{\mathbf{d}}(t)$. Formally,

$$\boldsymbol{x}_n(0) = \boldsymbol{x}_{\mathbf{d}}(0), \qquad \forall n \in \mathbb{N}. \tag{25}$$

On one hand, Assumption 1 is justified for switch-type actuators because their stroke is inherently constrained between two limiting positions, and their magnetic flux is limited due to magnetic saturation. On the other hand, Assumption 2 requires that each operation starts from a steady state, which is often achievable in practice due to sufficiently long intervals between operations. It also implies that the influence of remanent magnetization and other disturbances on the initial state is negligible, which is also reasonable for the studied class of actuators.

Assumption 3. The gap reluctance $\mathcal{R}_{\mathrm{g}}$ is a monotonically increasing function of the position, i.e.

$$\mathcal{R}_{\mathrm{g}}'(z) > 0, \qquad \forall z \in [z_{\min}, z_{\max}]. \tag{26}$$

Assumption 4. In their domain, the differential reluctance $\mathcal{R}_{\Delta i}$ (6) is bounded and differentiable, whereas the magnetic and passive forces F_{mag} and F_{pas} (13) are bounded and twice differentiable.

Assumption 5. The magnetic flux is bounded such that

$$\phi \in [\phi_{\min}, \phi_{\max}), \tag{27}$$

where $\phi_{\min}$ and $\phi_{\max}$ are strictly positive constants.

Assumption 3 implies that the magnetic force is always negative (i.e. attractive), as expected. Assumption 4 is also a reasonable imposition to the dynamical system, although it somewhat limits the possible models (e.g., a model with a passive force that changes discretely with respect to the position would not be valid and should be approximated with a smooth function). In contrast, Assumption 5 is a control imposition that greatly simplifies its design (note that negative values of the magnetic flux are completely unnecessary because the magnetic force is an even function of the magnetic flux). It also prevents crossing the singularity point $\phi = 0$, which is uncontrollable. In practice, this last imposition can be achieved by saturating negative currents to zero (e.g. with a diode).

3.2. Motion control design

The objective is to determine a sequence of input signals u_n that drives the output y_n to converge to the desired one y_{d}. Our control strategy is based on a first-order linear ILC, known for its surprising effectiveness even for of highly nonlinear and uncertain systems (Xu, 2011),

$$u_{n+1} = u_n + K_n\,(y_{\mathrm{d}} - y_n), \tag{28}$$

where $K_n \in \mathbb{R}$ represents the learning control gain, dependent on the iteration number n to allow adaptability. The convergence proof, rooted in Xu and Tan (2003), is supported by two lemmas, which are presented and proved hereunder:

Lemma 1. *There exists positive constant scalars c_1, c_2 and c_3 and positive constant vector $\boldsymbol{c_4}$ such that*

$$\|\boldsymbol{f}(\boldsymbol{x}_1, u_1) - \boldsymbol{f}(\boldsymbol{x}_2, u_2)\| \le c_1\big(\|\boldsymbol{x}_1 - \boldsymbol{x}_2\| + |u_1 - u_2|\big), \tag{29}$$

$$c_2 \le \partial h/\partial u \le c_3 \;\vee\; -c_2 \le \partial h/\partial u \le -c_3, \tag{30}$$

$$|\partial h/\partial \boldsymbol{x}| \le \boldsymbol{c_4}. \tag{31}$$

Proof. Firstly, from Assumptions 1 and 4, $\boldsymbol{f}$ is bounded and almost differentiable everywhere. The only non-differentiable points are the ones in which the magnetic flux derivative is zero (11), but they are continuous because

$$\lim_{\phi \to 0} \mathcal{R}_{\Delta i}\big(\mathcal{F}_i, \phi, \dot{\phi}\big)\,\dot{\phi} = \mathcal{R}_{\Delta i}\big(\mathcal{F}_i, \phi, 0\big)\,0 = 0. \tag{32}$$

Therefore, it is Lipschitz continuous, as stated in (29).

Secondly, from the output definition (17)–(24), its partial derivative with respect to the input can be expressed as

$$\frac{\partial h}{\partial u} = g_a(\boldsymbol{x}) = -\frac{1}{m}\,\mathcal{R}_{\mathrm{g}}'(z)\,\phi\, g_\phi, \tag{33}$$

where m and g_ϕ are positive constants, while $\mathcal{R}_{\mathrm{g}}'(z)$ and ϕ are positive and bounded (see Assumptions 3 and 5). Therefore, $\partial h/\partial u$ is always negative and bounded, proving (30).

Lastly, its gradient with respect to the state vector is composed by the following elements:

$$\partial h/\partial z = \varrho^3 + 3\,\varrho\,\partial f_v/\partial z + \partial f_a/\partial z + \partial g_a/\partial z, \tag{34}$$

$$\partial h/\partial v = 3\,\varrho^2 + 3\,\varrho\,\partial f_v/\partial v + \partial f_a/\partial v + \partial g_a/\partial v, \tag{35}$$

$$\partial h/\partial \phi = 3\,\varrho\,\partial f_v/\partial \phi + \partial f_a/\partial \phi + \partial g_a/\partial \phi, \tag{36}$$

$$\partial h/\partial \boldsymbol{\mathcal{F}} = \partial f_a/\partial \boldsymbol{\mathcal{F}}. \tag{37}$$

These partial derivatives depend on up to the first, second and third partial derivatives of $\mathcal{R}_{\Delta i}$, F_{pas} and $\mathcal{R}_{\mathrm{g}}$, respectively, as can be checked in (20)–(24). Because they are bounded (Assumption 4), $\partial h/\partial \boldsymbol{x}$ is also bounded, matching (31). □

Lemma 2. *For a certain desired output y_{d}, there exists a unique input u_{d} such that*

$$\dot{\boldsymbol{x}}_{\mathbf{d}} = \boldsymbol{f}(\boldsymbol{x}_{\mathbf{d}}, u_{\mathrm{d}}), \tag{38a}$$

$$y_{\mathrm{d}} = h(\boldsymbol{x}_{\mathbf{d}}, u_{\mathrm{d}}). \tag{38b}$$

Proof. In accordance to the proposed output definition (17), the desired output is defined based on the desired position trajectory z_d and its time derivatives,

$$y_\mathrm{d} = \varrho^3\, z_\mathrm{d} + 3\,\varrho^2\, v_\mathrm{d} + 3\,\varrho\, a_\mathrm{d} + \dot{a}_\mathrm{d}, \tag{39}$$

where v_d, a_d and $\dot{a}_\mathrm{d}$ denote the desired velocity, acceleration and jerk, respectively.

Then, the first and second elements of the state vector $\boldsymbol{x}_\mathbf{d}$ are the position z_d and velocity v_d, which are already defined. The third state variable is the magnetic flux ϕ_d, which can be derived from the acceleration definition (13),

$$\phi_\mathrm{d} = \sqrt{2\,\frac{F_\mathrm{pas}(z_\mathrm{d}, v_\mathrm{d}) - m\,a_\mathrm{d}}{\mathcal{R}'_\mathrm{g}(z_\mathrm{d})}}. \tag{40}$$

The solution is unique because the magnetic flux is restricted to positive values (Assumption 5).

The last state variables are the magnetomotive forces $\mathcal{F}_{\mathrm{d}i}$. Given that their initial values $\mathcal{F}_{\mathrm{d}i}(0)$ are unique (Assumption 2), and that the magnetic flux and therefore its time derivative $\dot{\phi}_\mathrm{d}$ are also unique, the magnetomotive forces $\mathcal{F}_{\mathrm{d}i}$ can be uniquely determined as the solutions of the following differential equations:

$$\dot{\mathcal{F}}_{\mathrm{d}i} = \mathcal{R}_{\Delta i}(\mathcal{F}_{\mathrm{d}i}, \phi_\mathrm{d}, \dot{\phi}_\mathrm{d})\,\dot{\phi}_\mathrm{d}. \tag{41}$$

Finally, the desired input is uniquely defined based on the jerk definition (19),

$$u_\mathrm{d} = \frac{\dot{a}_\mathrm{d} - f_a(\boldsymbol{x}_\mathbf{d})}{g_a(\boldsymbol{x}_\mathbf{d})}. \quad \square \tag{42}$$

Lastly, the convergence of the control law during motion is stated in the following proposition:

Proposition 1. *If the control action applied to the system (15) is computed from (28) while ensuring that the control gain K_n satisfies the following condition for every iteration n:*

$$K_\mathrm{min} \le K_n < 0, \qquad K_\mathrm{min} = -\frac{2\,m}{g_\phi \max\left(\mathcal{R}'_\mathrm{g}(z)\right)\phi_\mathrm{max}}, \tag{43}$$

then the position z_n tends to the desired trajectory z_d as the number of iterations n increases.

Proof. With a constant gain $K_n = K$, $\forall n$, and given Assumption 2 and Lemmas 1 and 2, the monotonic convergence of the input u toward u_d is theoretically guaranteed (Xu & Tan, 2003) if

$$|1 - K\,\partial h/\partial u| < 1. \tag{44}$$

Note that $\partial h/\partial u = g_a(\boldsymbol{x})$ and is always negative (33). After some manipulations,

$$2/g_a(\boldsymbol{x}) < K < 0. \tag{45}$$

Furthermore, from Assumption 5 as well as the definitions of g_a (21) and K_min (43), it follows that

$$\frac{2}{g_a(\boldsymbol{x})} = -\frac{2\,m}{g_\phi\,\mathcal{R}'_\mathrm{g}(z)\,\phi} > -\frac{2\,m}{g_\phi \max\left(\mathcal{R}'_\mathrm{g}(z)\right)\phi_\mathrm{max}} = K_\mathrm{min}. \tag{46}$$

Therefore, (43) is a sufficient condition to guarantee (44), and thus the input converges to u_d. Because the convergence is monotone for any constant $K \in [K_\mathrm{min}, 0)$, any sequence of adaptive gains $K_n \in [K_\mathrm{min}, 0)$ also guarantees said convergence. Moreover, given Lemma 2, the convergence toward u_d implies that the output tends to y_d and, more importantly, the position converges to the desired trajectory z_d. $\square$

Note that the controller has been designed based on the assumption of perfectly known dynamics. As previously stated, non-repeating disturbances can have an impact on the tracking performance because of the lack of real-time feedback. However, robustness against system uncertainties can be readily achieved by computing the gain bound K_min with the worst-case values of the model constants and functions. This involves considering the minimum value of m and the maximum values of g_ϕ, $\mathcal{R}'_\mathrm{g}(z)$ and ϕ_max. These minimum and maximum values should be derived from the physical tolerances of the actual devices. If this is not feasible, the parameter ranges can be estimated with an identification process of a sufficiently large sample of devices from the same family. In addition, it may be advisable to set the minimum and maximum values of these parameters conservatively, incorporating a margin or tolerance to account for other modeling errors and disturbances.

3.3. Full control design

The proposed control law (28) serves as the basis for the full controller. It is modified and expanded by accounting for some practical considerations and limitations. Firstly, it should be noted that the controller must be implemented separately for the opening and closing operations, but, for clarity, the distinction between operation types is omitted. Another important consideration is that, in a practical scenario, the time is discretized with a certain sampling period T, i.e. $t \in \{0, T, 2T, \ldots\}$, and that the time resets ($t = 0$) at the beginning of each iteration n.

Regarding the control law, it is separated into different intervals. During motion, the controller is defined as

$$u_{n+1}(t) = \bar{u}_n(t) + \Delta u_n(t), \qquad \forall t \in [t_0, t_\mathrm{f}], \tag{47}$$

where t_0 and t_f represent the initial and final instants of the motion interval, respectively, $\bar{u}_n(t)$ is the smoothed previous input, and Δu_n is the input variation based on the output error.

It is desirable to filter or smooth the input signal in order to eliminate high-frequency noise, especially so when using the input signal to estimate the position. A widely used measure in ILC applications is the smoothing of the previous input with a Q-filter in order to reduce sensitivity against high-frequency uncertainties. The proposed filter is formulated as

$$\bar{u}_n(t) = w\,u_n(t - T) + (1 - 2\,w)\,u_n(t) + w\,u_n(t + T), \tag{48}$$

where $w \in [0, 0.5]$ is the filter coefficient, which gives more weight to the previous and next samples as w increases. In this case, the Q-filter can be considered a weighted-average operator in a symmetrical window (Wang et al., 2009).

As an additional measure, the input variations are saturated in order to avoid large changes in the input between iterations, which may be caused by unrepeatable perturbations or errors. Formally, it is expressed as

$$\Delta u_n(t) = \mathrm{sat}_{-\Delta u_\mathrm{max}}^{+\Delta u_\mathrm{max}}\left(K_n\left(y_\mathrm{d}(t) - y_n(t)\right)\right), \tag{49}$$

where sat denotes the saturation function, ensuring that $\Delta u \in [-\Delta u_\mathrm{max}, \Delta u_\mathrm{max}]$, and K_n is the control parameter. The constant Δu_max should be chosen as a fraction of the maximum voltage.

Previous measures are quite general, and can be applied to many other ILC applications. In contrast, the following one is specifically intended for soft-landing control applications. Note that position tracking is not the ultimate objective, but rather a means to reduce impact velocities. Taking this into account, this paper proposes an adaptive control parameter,

$$K_n = \max\left(K_\mathrm{min}, -k\,\|\boldsymbol{v}_\mathbf{c}\|^2\right), \tag{50}$$

where k is a new control constant and $\boldsymbol{v}_\mathbf{c}$ is the vector of impact velocities in the previous iteration. Notice that it is saturated to K_min if lesser than that value to ensure that the condition (43) from Proposition 1 is satisfied.

Lastly, the controller should work for the full hybrid system, represented in Fig. 4, instead of only during the motion intervals. On one hand, before the motion, it is important to note that the coil must be energized or de-energized (in the closing or opening operation,

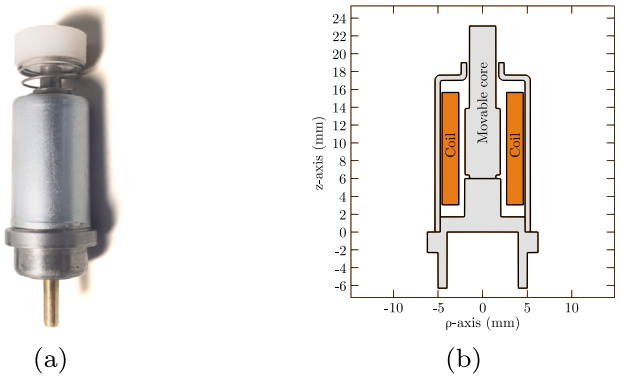

Fig. 5. Solenoid valve used for testing. (a) Photo. (b) Longitudinal section.

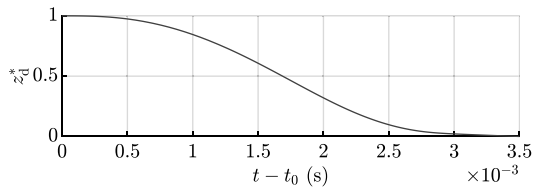

Fig. 6. Desired position trajectory for the closing operations.

respectively) so that at the motion start ($t = t_0$), the magnetic flux ϕ_0 is the necessary one to balance the magnetic and passive forces (13), i.e.

$$F_{\text{pas}}(z_0, 0) + F_{\text{mag}}(z_0, \phi_0) = 0, \tag{51}$$

where the initial position is $z_0 = z_{\max}$ or $z_0 = z_{\min}$, depending on the operation type (closing or opening, respectively). To achieve the previous condition at $t = t_0$, we propose to apply during an adaptive time interval a constant voltage u_{prev}, which should be large or small enough to ensure that the actuator can start separating from $z = z_{\max}$ or $z = z_{\min}$ in closing or opening operations, respectively. Formally,

$$u_{n+1}(t) = u_{\text{prev}}, \qquad \forall t \in [t_0 - \tau_{n+1},\, t_0), \tag{52}$$

where τ_{n+1} denotes the interval. It is iteratively updated as

$$\tau_{n+1} = \tau_n + c_\tau\,(t_{\text{takeoff}} - t_0), \tag{53}$$

being t_{takeoff} the instant in which the actuator started moving in the previous iteration and $c_\tau \in (0, 1]$ a filter coefficient. Intuitively, for larger c_τ, the interval is updated more aggressively, which is more suitable when cycle-to-cycle variability is low.

On the other hand, after the motion, the actuator must be kept in its final position. This is handled by applying a constant voltage u_{post}, which must be large or small enough to keep the actuator at $z = z_{\min}$ or $z = z_{\max}$ in closing or opening operations, respectively,

$$u_{n+1}(t) = u_{\text{post}}, \qquad \forall t > t_{\text{f}}. \tag{54}$$

4. Control application

4.1. Tested actuator and models

The proposed soft-landing control solution is tested with a commercial linear-travel solenoid valve, shown in Fig. 5. The cylindrically symmetrical core consists of a fixed part and a plunger. The current through the coil generates a magnetic force that tends to attract the movable core toward the fixed core, whereas the spring force tends to keep them separated.

Two specific models of this device are used. Both follow the general structure presented in Section 2, but with different complexities. The first one is the complete model, which was previously proposed (Moya-Lasheras et al., 2021) and is summarized in Appendix A. It includes the most important electromagnetic phenomena: magnetic saturation, hysteresis, eddy currents and flux fringing. Thus, it is chosen for emulating the real system in the simulated analyses. However, this model is too complex for control of simple reluctance actuators. For one, given the large number of parameters, the model identification is computationally expensive. This is especially critical when working with low-cost actuators with large unit-to-unit variability, because parameters should be recalculated for each device. Moreover, the implementation cost of controllers and estimators based on this model is usually prohibitive.

Therefore, for estimation and control, we propose to use a simplified model, summarized in Appendix B. In contrast to the previous one, this model neglects the complex magnetic hysteresis phenomenon. It has been previously designed for position estimation of reluctance actuators (Moya-Lasheras et al., 2022). It is also suitable for position tracking control with the proposed formulation in Section 3. The model structure is a particularization of the general form presented in Section 2, but with some constant and variable changes to reduce the complexity and the number of parameters. Mainly, the state variables are modified as follows:

$$z^* = z/z_{\max}, \qquad v^* = v/z_{\max}, \qquad \phi^* = N\,\phi, \tag{55}$$

where z^* is the normalized position, such that $z^* \in [0,\, 1]$; v^* is its time derivative; and ϕ^* is the flux linkage, replacing the magnetic flux as the third state variable.

The parameter values of the complete and simplified models, presented in Tables 1 and 2, respectively, have been obtained through an identification procedure. This process minimizes simulated errors with respect to experimental position, voltage, and current signals measured from the real device. As an indicator of the accuracy of each model, the simulated current has a normalized root mean square error of 2.99% with the complete model and 5.74% with the simplified model.

Table 1
Parameters of the complete model.

Symbol	Value	Symbol	Value
R	50 Ω	$\mathcal{R}_{\text{g},0}$	$2.58 \cdot 10^{9}\ \text{H}^{-1}$
N	1200	$\mathcal{R}'_{\text{g},0}$	$7.37 \cdot 10^{10}\ \text{H}^{-1}/\text{m}$
l_{c}	0.055 m	k_1	$334\ \text{m}^{-1}$
A_{c}	$1.26 \cdot 10^{-5}\ \text{m}^2$	k_2	0.154 m
k_{eddy}	$1440\ \Omega^{-1}$	m	$1.20 \cdot 10^{-3}$ kg
M_{sat}	$2.90 \cdot 10^{6}$ A/m	k_{sp}	52.1 N/m
b	$3.66 \cdot 10^{-3}$ T	z_{sp}	0.0161 m
c	0.724	c_{f}	0.0375 N s/m
κ	668 A/m	$z_{\min}$	0
α	0.426	$z_{\max}$	$1 \cdot 10^{-3}$ m

Table 2
Parameters of the simplified model.

Symbol	Value	Symbol	Value
$\mathcal{R}^*_{\text{g},0}$	$4.51\ \text{H}^{-1}$	ϕ^*_{sat}	0.0276 Wb
$\mathcal{R}'^*_{\text{g},0}$	$51.2\ \text{H}^{-1}$	m^*	$1.20 \cdot 10^{-9}\ \text{kg m}^2$
k^*_1	0.334	k^*_{sp}	$5.21 \cdot 10^{-5}$ N m
k^*_2	154	z^*_{sp}	16.1
$\mathcal{R}^*_{\text{c},0}$	$3.23\ \text{H}^{-1}$	c^*_{f}	$3.75 \cdot 10^{-8}$ N m s

4.2. Control strategy

The control strategy proposed in Section 3.3 is particularized to the presented actuator. Firstly, the desired position trajectory for the closing operations has been designed through an optimal control method proposed in Moya-Lasheras et al. (2020b), using the simplified model with the nominal parameter values (see Table 2). The result is presented in Fig. 6.

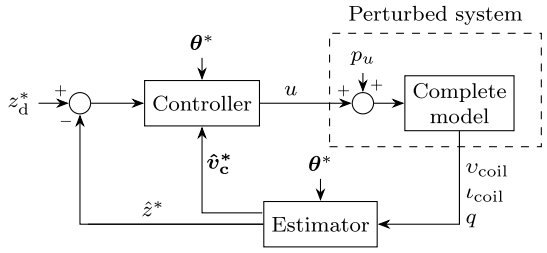

Fig. 7. Control and estimation diagram.

Then, the control diagram is depicted in Fig. 7. The actuator dynamics is represented by the dashed box, whose input is the control action u and outputs are the measurements of voltage v_{coil}, current ι_{coil} and the discrete state q. For the simulated cases, the complete model (Appendix A) is used, and random voltage perturbations p_u are also introduced.

In this practical scenario, the controller does not rely on direct position measurements. Instead, it uses estimates of the position $\hat{z}^*$ and the vector of contact velocities $\hat{\boldsymbol{v}}_c^*$ from the previous iteration. These estimates are derived from measurements of voltage v_{coil}, current ι_{coil} and the discrete state q. We employ an offline estimator based on the simplified model (Appendix B), as proposed in Moya-Lasheras et al. (2022). The estimator uses an Extended Rauch–Tung–Striebel two-pass smoother, performing a forward pass with an Extended Kalman filter, followed by backward pass covering the entire operation interval. The backward pass improves greatly the estimation accuracy, as demonstrated by simulated and experimental analyses (Moya-Lasheras et al., 2022). However, it renders the estimator unsuitable for real-time implementation. Fortunately, the proposed controller, intentionally designed without a real-time feedback loop (47)–(54), allows the position to be obtained offline or iteratively.

Both the controller and estimator depend on a vector of parameters from the simplified model. It is defined as

$$\boldsymbol{\theta}^* = \begin{bmatrix} m^* & k_{sp}^* & z_{sp}^* & c_f^* & \mathcal{R}_{g,0}^* & \mathcal{R}'^*_{g,0} & k_1^* & k_2^* & \mathcal{R}_{c,0}^* & \phi_{sat}^* \end{bmatrix}^\top, \tag{56}$$

where the asterisk superscript is used to make a distinction between these auxiliary parameters (obtained through normalization and other manipulations) and the ones from the complete model.

5. Results

5.1. Simulated analysis

Multiple simulations are performed to analyze the performance of the controller and the estimator. To emulate unit-to-unit variability, the model parameters are perturbed in each run. Formally,

$$\theta_i^* = \theta_i^{*\text{nom}} (1 + e_{\theta i}), \tag{57}$$

where θ_i^* is the ith component of the parameter vector (56), $\theta_i^{*\text{nom}}$ is the corresponding nominal parameter value (Table 2) and $e_{\theta i}$ is the relative error. Each relative error is a realization of a uniform random variable E_θ,

$$E_\theta \sim \mathcal{U}\left(-\delta_\theta/2,\, \delta_\theta/2\right), \tag{58}$$

where δ_θ denotes its interval length.

Moreover, cycle-to-cycle variability is emulated by perturbing the voltage in each iteration n. Formally, the applied voltage is $u_n(t) + p_u$, where $u_n(t)$ is the control action computed based on the proposed method in Section 3.3; and p_u represents the voltage perturbation (see Fig. 7), which is a realization of a normal random variable P_u,

$$P_u \sim \mathcal{N}\left(0,\, {\sigma_u}^2\right), \tag{59}$$

whose standard deviation is set to $\sigma_u = 0.025\,\text{V}$.

Regarding the control algorithm, it has been initialized with a constant voltage, $u_1(t) = 30\,\text{V}$. This uncontrolled first commutation serves also as a reference to assess the improvement in following iterations. The voltage values before and after the motion are accordingly set as $u_{prev} = u_{post} = 30\,\text{V}$. Moreover, the control gain K_{min} is specified based on the proposed definition (43) with a conservative adjustment to account for potential modeling errors,

$$K_{min} = \max\left(\frac{-2\,m^*}{\mathcal{R}'^*_{g,0}\,\phi_{sat}^*}\right) = \frac{-2\,m^{*\text{nom}}\,(1+\delta_\theta)}{\mathcal{R}'^{*\text{ nom}}_{g,0}\,\phi_{sat}^{*\text{ nom}}\,(1-\delta_\theta)^2}. \tag{60}$$

The remaining control constants ϱ, w, Δu_{max}, k and c_τ are not based on the model, so they are optimized for each case separately in order to improve the control performance.

Four Monte Carlo tests have been performed for different parameter errors ($\delta_\theta = 5$, 10, 20 and 50%). For each one, 500 runs are carried out, with 100 commutations or iterations. This number of operations has been selected to show the control convergence, but note that this controller has been designed for working indefinitely in practical scenarios.

The results are summarized in Fig. 8. The top graphs display the distribution of the absolute values of the position estimation errors, $|\tilde{z}^*| = |z^* - \hat{z}^*|$, in each iteration n. Note that the position errors while resting at one of the limiting positions ($q = 1$ or $q = 3$) are always zero, so only the errors during motion ($q = 2$) have been computed. Note also that $z^* \in [0, 1]$, so the errors are significant but still quite small considering that the estimator relies on a simplified model with parameter errors. As expected, the estimation errors increase with larger parameter errors, especially in the last case, in which $\delta_\theta = 50\%$. But the estimator is demonstrated to be quite robust, because the errors increase at a smaller rate than the parameters, e.g., increasing ten times the parameter errors (from $\delta_\theta = 5\%$ to 50%) increases the errors about five times.

The position estimation allows tracking it via the proposed ILC, but the ultimate objective is to decrease the impact velocities. Thus, to check the control performance, an equivalent contact velocity $v_{c,eq}$ is calculated in each commutation, having the same total kinetic energy as all contact velocities,

$$v_{c,eq} = \|\boldsymbol{v}_c\|. \tag{61}$$

These velocities are summarized in the bottom graphs of Fig. 8. For $\delta_\theta = 5$, 10 and 20%, the results are very similar, despite their different position estimation errors. This shows that the control is quite robust to estimation errors. The root mean square velocities in the last iterations ($n > 50$) are 0.181, 0.206 and 0.214 m/s, respectively, which are less than 2% of the average impact energy in the uncontrolled scenarios ($n = 1$). In the last case, in which $\delta_\theta = 50\%$, there is a significant increase in the estimation errors, which results in a significantly slower convergence speed of the control. In any case, after 50 iterations, the results are still very good, with a root mean square velocity of 0.26 m/s. Therefore, the control is effective even in the undesired scenarios in which the model is not properly identified.

Moreover, for comparison purposes, a state-of-the-art run-to-run (R2R) control (Moya-Lasheras & Sagues, 2020) is also simulated under the same conditions. This strategy uses a Bayesian optimization algorithm for adapting the model parameters in each iteration—which are used to calculate the current applied to the actuator. Conforming with the cited paper, the optimization cost is defined as the equivalent contact velocity (61) squared. However, in this case, the impact velocities are estimated. For consistency, all R2R control parameters have been adjusted following the same methods as the cited work. Fig. 9 shows equivalent contact velocities from this alternative controller, which have been obtained following the same procedure. For increasing parameter errors, the results worsen, especially the variability. Ultimately, for every case they are considerably worse than the results from

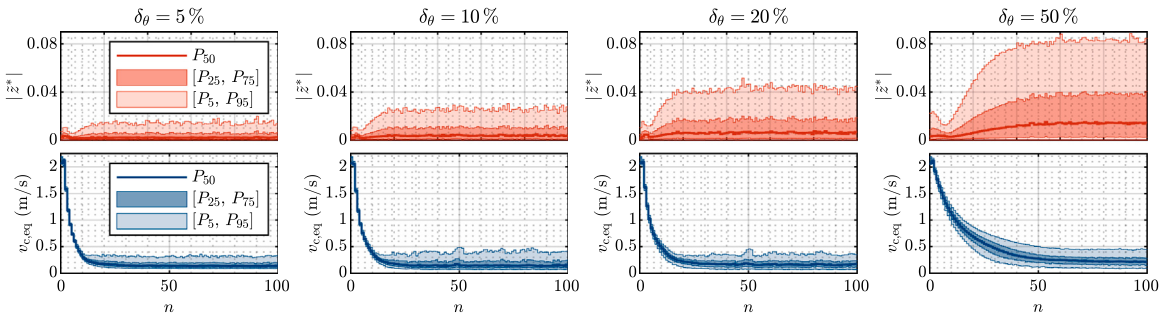

Fig. 8. Distribution of the position estimation errors (top) and equivalent contact velocities (bottom) for different parameter errors with the proposed controller. The graphs include the median value (P_{50}), the interquartile range ($[P_{25},\ P_{75}]$) and the 5th to 95th percentile interval ($[P_5,\ P_{95}]$).

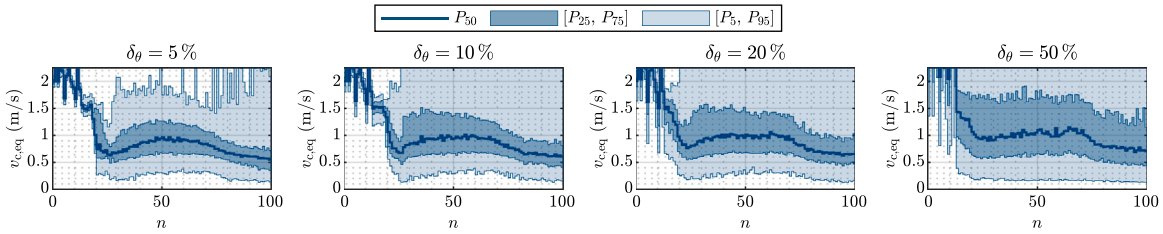

Fig. 9. Distribution of equivalent contact velocities for different parameter errors with an alternative state-of-the-art controller. The graphs include the median value (P_{50}), the interquartile range ($[P_{25},\ P_{75}]$) and the 5th to 95th percentile interval ($[P_5,\ P_{95}]$).

the proposed controller. As the run-to-run control uses the estimated impact velocities v_c^* for evaluating each iteration and then adapt the parameters, it is quite sensitive to the estimation errors, even when they are relatively small ($\delta_\theta = 5\%$).

5.2. Experimental validation

The proposed control strategy is validated with the experimental setup shown in Fig. 10, in which the equipment has been labeled as follows:

1. The actuator described in Section 4.1 (Fig. 10(b))
2. Personal computer
3. Power supplies (Tenma 72-10505)
4. Voltage amplifier
5. USB oscilloscope with an arbitrary waveform generator (Pico-Scope 4824)
6. High-speed and high-accuracy laser displacement sensor head (LK-H082)
7. Displacement sensor controller (Keyence LK-G5001P)

The voltage signals that are supplied to the actuator coil are designed in the PC with MATLAB, generated by the USB oscilloscope and then amplified. The oscilloscope also measures the coil voltage, current (with a shunt resistor) and the plunger position (through the displacement sensor), and sends them to the computer. Note that the position measurements are not used in the implemented solution, but in the validation of the estimation and control.

The controller is initialized and executed 100 times, in the same manner as in Section 5.1. To account for modeling errors, the constant $K_{\min}$ (60) is determined by assuming that $\delta_\theta = 10\%$, which is considered sufficiently large. The resulting equivalent contact velocities are condensed in Fig. 11. They are similar to the ones from the simulated analysis, with a root mean square velocity of 0.37 m/s in the last iterations ($n > 50$), which corresponds to a 94.3% average reduction of the impact energy with respect to the uncontrolled cases ($n = 1$). Also, we can see that the controller is quite fast, needing about 20 operations to converge, which is in agreement with the simulated results with $\delta_\theta = 10\%$.

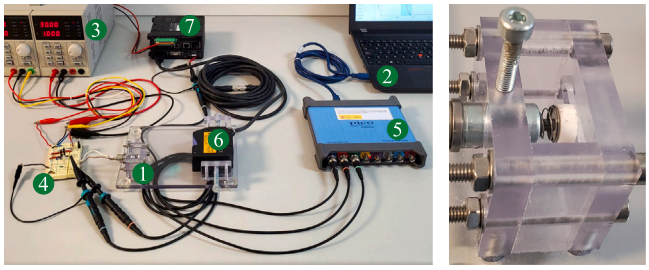

Fig. 10. Experimental setup. (a) Equipment. (b) Actuator.

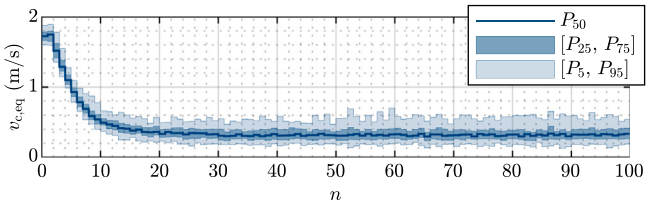

Fig. 11. Experimental results using the proposed ILC. Distribution of equivalent contact velocities with respect to the iteration number.

As explained in Section 3.3, the control gain is adapted in each iteration based on the previous impact velocities. To study its evolution, the obtained values are displayed in Fig. 12. The left-hand graph represents the distribution of values of $-k\,\|\hat{\boldsymbol{v}}_c^*\|^2$, which is the adapted parameter K_n before the saturation. Note that the values in the first iteration are larger than $K_{\min}$ and thus are saturated to said value in order to ensure the theoretical tracking convergence (see Proposition 1). Note also that this control parameter is based on the estimated contact velocities. To show that estimation errors do not have a strong impact on the control parameter, the right-hand graph displays the distribution of values of $-k\,\|\boldsymbol{v}_c^*\|^2$, which would be the adapted parameter K_n after saturation if the real contact velocities were available. There seems to be a very slight underestimation of the contact velocities, as these ideal values

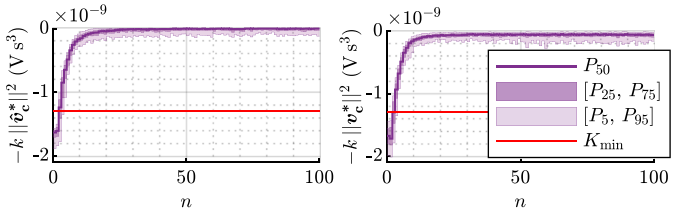

Fig. 12. Adaptive control parameter values (before saturation to $K_{\min}$) with respect to the iteration number: real values obtained from estimated impact velocities and used in the control (left), and ideal values obtained from measured impact velocities (right).

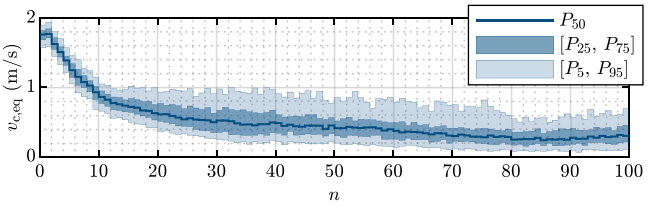

Fig. 13. Experimental results using an ILC with a fixed gain. Distribution of equivalent contact velocities with respect to the iteration number.

have greater magnitudes than the ones used in the control. Nonetheless, they are very similar, making the effect of these mismatches in the control performance insignificant.

The effectiveness of the proposed adaptive ILC gain is assessed by comparing it to a strategy using a fixed gain, obtained as the average gain from the prior experiment ($K \approx -10^{-10}$ V s^3). An experiment is performed under the same conditions, resulting in equivalent contact velocities that are summarized in Fig. 13. In contrast to the proposed solution (Fig. 11), the fixed gain ILC exhibits a considerably slower convergence, a consequence of the higher absolute value of the adapted gain during the initial iterations. Additionally, it displays a higher overall variability, particularly noticeable from the 20th iteration onward. This behavior can be attributed to the higher magnitude of the fixed gain during those iterations. This comparison underscores the advantages of employing an adaptive gain ILC strategy over a fixed gain counterpart.

The two control strategies are further compared by depicting the obtained position trajectories in the 1st, 10th, and 100th iterations (Fig. 14). The top graphs correspond to the proposed adaptive control strategy, while the bottom graphs are from the fixed gain alternative. These specific operations were selected from the 100 repetitions because each one has the closest equivalent contact velocity to its corresponding average. The measured position (exp.) is normalized for a direct comparison with the estimated one (est.), which is the one used by the controller to track the reference trajectory (ref.). Notably, estimation errors are consistently small, but in some cases they are noticeable.

The left-hand graphs of Fig. 14 display the position trajectories of the first iteration for both control strategies, where a constant voltage is applied, resulting in trajectories with high impact velocities. Despite the identical input signal, the position trajectories are noticeably distinct, underscoring the inherent cycle-to-cycle variability in the device, a primary challenge in its control. Moving to the middle graphs, the trajectories in the 10th iteration are presented. The proposed control strategy effectively tracks the estimated position in the initial part of the motion interval (top graph), while the alternative strategy lags significantly (bottom graph). Finally, the right-hand graphs depict the trajectories in the last iteration. With the proposed control strategy, there are small estimation and tracking errors at the end of the motion interval. Consequently, perfect soft landing is not achieved, but the impact velocity is considerably reduced. The alternative strategy exhibits a similar behavior, with slightly larger tracking errors and impact velocity.

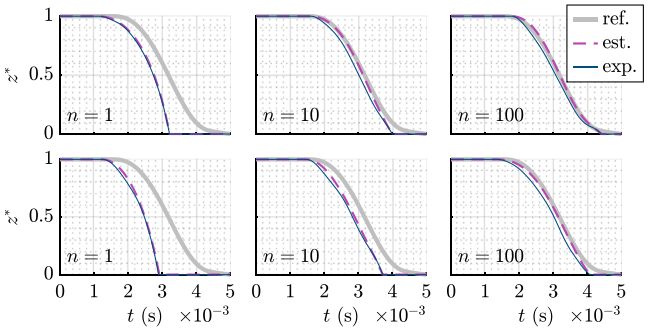

Fig. 14. Representative experimental results with adaptive (top) and fixed (bottom) gains: 1st (left), 10th (middle) and 100th (right) iterations.

6. Conclusion

A new iterative learning controller has been proposed for position tracking and soft landing of reluctance actuators, aiming to improve switching operation performance. The controller operates without a real-time feedback loop, making it sensitive to non-repeating perturbations. Despite this limitation, it offers valuable advantages for applications involving inexpensive or fast-switching actuators, where the implementation of high-frequency position observers or sensors in real-time is impractical. It is especially useful in situations where position estimates can be obtained offline, after each operation. Offline estimators offer two significant advantages over their real-time counterparts: reduced implementation costs and increased accuracy. This improved accuracy can be attributed to the process of refining the estimated state at a given time by using posterior observation samples.

The proposed controller is validated with simulated and experimental analyses. Despite the absence of a feedback controller and the presence of significant estimation errors, the control performance is remarkably good. Additionally, the comparison with a fixed-gain ILC highlights the advantages of the proposed gain adaptation, including faster convergence and reduced variability in the control results.

CRediT authorship contribution statement

Eduardo Moya-Lasheras: Writing – original draft, Visualization, Validation, Software, Methodology, Investigation, Formal analysis, Data curation, Conceptualization. **Carlos Sagues:** Writing – review & editing, Supervision, Project administration, Funding acquisition.

Declaration of competing interest

The authors declare that they have no known competing financial interests or personal relationships that could have appeared to influence the work reported in this paper.

Acknowledgments

This work was supported in part via grants PID2021-124137OB-I00, TED2021-130224B-I00, and CPP2021-008938, funded by MCIN/AEI/10.13039/501100011033 and by ERDF A way of making Europe; and in part by the Government of Aragón (grant T45_23R).

Appendix A. Complete model

This appendix provides a concise summary of a dynamical model for short-stroke reluctance actuators, firstly presented in Moya-Lasheras et al. (2021). It is adapted here to demonstrate that it is a particularization of the generalized dynamical description from Section 2.

Specifically, the passive force F_{pas} (13), the gap reluctance $\mathcal{R}_{\text{g}}$ (4) and the differential reluctance $\mathcal{R}_{\Delta}$ (6) are defined as follows:

$$F_{\text{pas}}(z, v) = k_{\text{sp}}\,(z_{\text{sp}} - z) - c_{\text{f}}\,v, \tag{A.1}$$

$$\mathcal{R}_{\text{g}}(z) = \mathcal{R}_{\text{g},0} + \frac{\mathcal{R}'_{\text{g},0}\,z}{1 + k_1\,z\,\ln(k_2/z)}, \tag{A.2}$$

$$\mathcal{R}_{\Delta}(\mathcal{F}_{\text{c}}, \phi, \dot{\phi}) = \frac{l_{\text{c}}}{A_{\text{c}}}\left(\frac{1}{\mu_0} - \frac{\mathrm{d}M_{\text{c}}}{\mathrm{d}B_{\text{c}}}\left(\mathcal{F}_{\text{c}}, \phi, \operatorname{sgn}\dot{\phi}\right)\right), \tag{A.3}$$

where $\mu_0 \approx 4\pi\cdot 10^{-7}$ H/m is the magnetic permeability of free space, and k_{sp}, z_{sp}, c_{f}, $\mathcal{R}_{\text{g},0}$, $\mathcal{R}'_{\text{g},0}$, k_1, k_2, l_{c} and A_{c} are positive constants to be fitted.

Moreover, $\mathrm{d}M_{\text{c}}/\mathrm{d}B_{\text{c}}$ is a function based on the Jiles–Atherton magnetic hysteresis model, depending on additional positive parameters (α, M_{sat}, b, κ and c).

Appendix B. Simplified model

This appendix discusses a simplified model, initially presented in Moya-Lasheras et al. (2022). This model introduces parameter and variable changes in order to reduce its complexity, but it can be shown that it is still a particularization of the general model from Section 2. For clarity, different notation is used for the auxiliary state variables (55) and model parameters.

In this case, the passive force F^*_{pas} (13) and the gap reluctance $\mathcal{R}^*_{\text{g}}$ (4) follow the same structure than their complete model counterparts (A.2) and (A.1), but with different parameters. It is worth noting that these new parameters are related to those of the complete model as follows:

$$\begin{aligned}
N^* &= 1, & z^*_{\max} &= 1,\\
\mathcal{R}^*_{\text{g},0} &= \mathcal{R}_{\text{g},0}/N^2, & m^* &= m\,{z_{\max}}^2,\\
\mathcal{R}'^*_{\text{g},0} &= \mathcal{R}'_{\text{g},0}\,z_{\max}/N^2, & k^*_{\text{sp}} &= k_{\text{sp}}\,{z_{\max}}^2,\\
k^*_1 &= k_1\,z_{\max}, & z^*_{\text{sp}} &= z_{\text{sp}}/z_{\max},\\
k^*_2 &= k_2/z_{\max}, & c^*_{\text{f}} &= c_{\text{f}}\,{z_{\max}}^2.
\end{aligned} \tag{B.1}$$

On the other hand, the differential reluctance $\mathcal{R}^*_{\Delta}$ (6) is defined differently. The simplified magnetomotive force, $\mathcal{F}^*$ is introduced as a scaled version of the standard one, $\mathcal{F}^* = \mathcal{F}/N$, and is expressed as a function of the flux linkage ϕ^*, based on a modified version of the Fröhlich–Kennelly magnetic saturation model,

$$\mathcal{F}^* = \mathcal{F}^*(\phi^*) = \frac{\mathcal{R}^*_{\text{c},0}\,\phi^*}{1 - |\phi^*|/\phi^*_{\text{sat}}}. \tag{B.2}$$

Then, to show its link to the generalized model, the differential reluctance can be easily derived as follows:

$$\mathcal{R}^*_{\Delta}(\mathcal{F}, \phi, \dot{\phi}) = \frac{\mathrm{d}\mathcal{F}^*}{\mathrm{d}\phi^*} = \frac{\mathcal{R}^*_{\text{c},0}\,{\phi^*_{\text{sat}}}^2}{\left(\phi^*_{\text{sat}} - |\phi^*|\right)^2}. \tag{B.3}$$

References

Bao, J., Vrijsen, N. H., Gysen, B. L. J., Sprangers, R. L. J., & Lomonova, E. A. (2014). Optimization of the force density for medium-stroke reluctance actuators. *IEEE Transactions on Industry Applications*, *50*(5), 3194–3202. http://dx.doi.org/10.1109/TIA.2014.2304586.

Benosman, Mouhacine, & Atinç, Gökhan M. (2015). Extremum seeking based adaptive control for electromagnetic actuators. *International Journal of Control*, *88*(3), 517–530. http://dx.doi.org/10.1080/00207179.2014.964779.

Braun, Tristan, Reuter, Johannes, & Rudolph, Joachim (2019). Observer design for self-sensing of solenoid actuators with application to soft landing. *IEEE Transactions on Control Systems Technology*, *27*(4), 1720–1727. http://dx.doi.org/10.1109/TCST.2018.2821656.

Bristow, Douglas A., & Alleyne, Andrew G. (2008). Monotonic convergence of iterative learning control for uncertain systems using a time-varying filter. *IEEE Transactions on Automatic Control*, *53*(2), 582–585. http://dx.doi.org/10.1109/TAC.2007.914252.

Chien, Chiang-Ju, & Tayebi, Abdelhamid (2008). Further results on adaptive iterative learning control of robot manipulators. *Automatica*, *44*(3), 830–837. http://dx.doi.org/10.1016/j.automatica.2007.06.023.

Chladny, Ryan R., & Koch, Charles R. (2008). Flatness-based tracking of an electromechanical variable valve timing actuator with disturbance observer feedforward compensation. *IEEE Transactions on Control Systems Technology*, *16*(4), 652–663. http://dx.doi.org/10.1109/TCST.2007.912121.

Di Bernardo, M., Santini, S., Di Gaeta, Alessandro, Hoyos Velasco, C. I., & Montanaro, U. (2012). Model-based soft landing control of an electromechanical engine valve actuator. *vol. 2*, In *Dynamic systems and control conference* (pp. 87–94). Fort Lauderdale, Florida, USA: American Society of Mechanical Engineers Digital Collection, http://dx.doi.org/10.1115/DSCC2012-MOVIC2012-8526.

Di Gaeta, Alessandro, Hoyos Velasco, Carlos I., & Montanaro, Umberto (2015). Cycle-by-cycle adaptive force compensation for the soft-landing control of an electro-mechanical engine valve actuator. *Asian Journal of Control*, *17*(5), 1707–1724. http://dx.doi.org/10.1002/asjc.988.

Gill, Rajan, Wahrburg, Arne, Craciun, Octavian, Listmann, Kim, & Reuber, Christian (2015). Model based landing control for a bistable electromagnetic actuator with discontinuous dynamics. In *2015 IEEE conference on control applications (CCA)* (pp. 1479–1485). Sydney, Australia: http://dx.doi.org/10.1109/CCA.2015.7320820.

Hoffmann, Wolfgang, Peterson, Katherine, & Stefanopoulou, Anna G. (2003). Iterative learning control for soft landing of electromechanical valve actuator in camless engines. *IEEE Transactions on Control Systems Technology*, *11*(2), 174–184. http://dx.doi.org/10.1109/TCST.2003.809242.

Huang, Deqing, Chen, Yong, Meng, Deyuan, & Sun, Pengfei (2021). Adaptive iterative learning control for high-speed train: A multi-agent approach. *IEEE Transactions on Systems, Man, and Cybernetics: Systems*, *51*(7), 4067–4077. http://dx.doi.org/10.1109/TSMC.2019.2931289.

Ito, Shingo, Troppmair, Stefan, Lindner, Bernhard, Cigarini, Francesco, & Schitter, Georg (2019). Long-range fast nanopositioner using nonlinearities of hybrid reluctance actuator for energy efficiency. *IEEE Transactions on Industrial Electronics*, *66*(4), 3051–3059. http://dx.doi.org/10.1109/TIE.2018.2842735.

Kahveci, Nazli E., & Kolmanovsky, Ilya V. (2010). Control design for electromagnetic actuators based on backstepping and landing reference governor. In *5th IFAC Symposium on Mechatronic Systems vol. 43*(18), 393–398. http://dx.doi.org/10.3182/20100913-3-US-2015.00051.

Katalenic, Andelko, Butler, Hans, & van den Bosch, Paul P. J. (2016). High-precision force control of short-stroke reluctance actuators with an air gap observer. *IEEE/ASME Transactions on Mechatronics*, *21*(5), 2431–2439. http://dx.doi.org/10.1109/TMECH.2016.2569023.

Ketelhut, Maike, Stemmler, Sebastian, Gesenhues, Jonas, Hein, Marc, & Abel, Dirk (2019). Iterative learning control of ventricular assist devices with variable cycle durations. *Control Engineering Practice*, *83*, 33–44. http://dx.doi.org/10.1016/j.conengprac.2018.10.012.

Kluk, Daniel J., Boulet, Michael T., & Trumper, David L. (2012). A high-bandwidth, high-precision, two-axis steering mirror with moving iron actuator. *Mechatronics*, *22*(3), 257–270. http://dx.doi.org/10.1016/j.mechatronics.2012.01.008.

Li, Xuefang, Shen, Dong, & Xu, Jian-Xin (2019). Adaptive iterative learning control for MIMO nonlinear systems performing iteration-varying tasks. *Journal of the Franklin Institute*, *356*(16), 9206–9231. http://dx.doi.org/10.1016/j.jfranklin.2019.08.012.

Lim, Hong Sun, Krishnan, R., & Lobo, N. S. (2008). Design and control of a linear propulsion system for an elevator using linear switched reluctance motor drives. *IEEE Transactions on Industrial Electronics*, *55*(2), 534–542. http://dx.doi.org/10.1109/TIE.2007.911942.

Lu, X.-D., & Trumper, D. L. (2005). Ultrafast tool servos for diamond turning. *CIRP Annals*, *54*(1), 383–388. http://dx.doi.org/10.1016/S0007-8506(07)60128-0.

Mercorelli, Paolo (2012). An antisaturating adaptive preaction and a slide surface to achieve soft landing control for electromagnetic actuators. *IEEE/ASME Transactions on Mechatronics*, *17*(1), 76–85. http://dx.doi.org/10.1109/TMECH.2010.2089467.

Moore, Kevin L., Chen, YangQuan, & Bahl, Vikas (2005). Monotonically convergent iterative learning control for linear discrete-time systems. *Automatica*, *41*(9), 1529–1537. http://dx.doi.org/10.1016/j.automatica.2005.01.019.

Moya-Lasheras, Eduardo, Ramirez-Laboreo, Edgar, & Sagues, Carlos (2020a). Model-free sliding-mode controller for soft landing of reluctance actuators. *IFAC-PapersOnLine*, *53*(2), 6256–6261. http://dx.doi.org/10.1016/j.ifacol.2020.12.1738.

Moya-Lasheras, Eduardo, Ramirez-Laboreo, Edgar, & Sagues, Carlos (2020b). Probability-based optimal control design for soft landing of short-stroke actuators. *IEEE Transactions on Control Systems Technology*, *28*(5), 1956–1963. http://dx.doi.org/10.1109/TCST.2019.2918479.

Moya-Lasheras, Eduardo, & Sagues, Carlos (2020). Run-to-run control with Bayesian optimization for soft landing of short-stroke reluctance actuators. *IEEE/ASME Transactions on Mechatronics*, *25*(6), 2645–2656. http://dx.doi.org/10.1109/TMECH.2020.2987942.

Moya-Lasheras, Eduardo, Sagues, Carlos, & Llorente, Sergio (2021). An efficient dynamical model of reluctance actuators with flux fringing and magnetic hysteresis. *Mechatronics*, *74*, Article 102500. http://dx.doi.org/10.1016/j.mechatronics.2021.102500.

Moya-Lasheras, Eduardo, Sagues, Carlos, Ramirez-Laboreo, Edgar, & Llorente, Sergio (2017). Nonlinear bounded state estimation for sensorless control of an electromagnetic device. In *2017 IEEE 56th annual conference on decision and control (CDC)* (pp. 5050–5055). Melbourne, Australia: http://dx.doi.org/10.1109/CDC.2017.8264407.

Moya-Lasheras, Eduardo, Schellekens, Jan M., & Sagues, Carlos (2022). Rauch–Tung–Striebel smoother for position estimation of short-stroke reluctance actuators. *IEEE Transactions on Control Systems Technology*, *30*(4), 1641–1653. http://dx.doi.org/10.1109/TCST.2021.3120909.

Owens, D. H., & Munde, G. S. (1998). Universal adaptive iterative learning control. *vol. 1*, In *Proceedings of the 37th IEEE conference on decision and control (cat. no.98CH36171)* (pp. 181–185). http://dx.doi.org/10.1109/CDC.1998.760618.

Pedersen, Henrik C., Bak-Jensen, Terkil, Jessen, Rasmus H., & Liniger, Jesper (2022). Temperature-independent fault detection of solenoid-actuated proportional valve. *IEEE/ASME Transactions on Mechatronics*, *27*(6), 4497–4506. http://dx.doi.org/10.1109/TMECH.2022.3158483.

Peterson, Katherine S., & Stefanopoulou, Anna G. (2004). Extremum seeking control for soft landing of an electromechanical valve actuator. *Automatica*, *40*(6), 1063–1069. http://dx.doi.org/10.1016/j.automatica.2004.01.027.

Ramirez-Laboreo, Edgar (2019). *Modeling and control of reluctance actuators* (Ph.D. thesis), Universidad de Zaragoza, URL https://zaguan.unizar.es/record/108263.

Ramirez-Laboreo, Edgar, Sagues, Carlos, & Llorente, Sergio (2017). A new run-to-run approach for reducing contact bounce in electromagnetic switches. *IEEE Transactions on Industrial Electronics*, *64*(1), 535–543. http://dx.doi.org/10.1109/TIE.2016.2605622.

Rotariu, Iuliana, Steinbuch, Maarten, & Ellenbroek, Rogier (2008). Adaptive iterative learning control for high precision motion systems. *IEEE Transactions on Control Systems Technology*, *16*(5), 1075–1082. http://dx.doi.org/10.1109/TCST.2007.906319.

Sa-e, Sakariya, Freeman, Christopher T., & Yang, Kai (2020). Iterative learning control of functional electrical stimulation in the presence of voluntary user effort. *Control Engineering Practice*, *96*, Article 104303. http://dx.doi.org/10.1016/j.conengprac.2020.104303.

Tai, Chun, & Tsao, Tsu-Chin (2003). Control of an electromechanical actuator for camless engines. *vol. 4*, In *Proceedings of the American control conference* (pp. 3113–3118). http://dx.doi.org/10.1109/acc.2003.1244007.

Upadhyay, Divyadeep, & Schaal, Christoph (2020). Optimizing the driving trajectories for guided ultrasonic wave excitation using iterative learning control. *Mechanical Systems and Signal Processing*, *144*, Article 106876. http://dx.doi.org/10.1016/j.ymssp.2020.106876.

Vrijsen, N. H., Jansen, J. W., & Lomonova, E. A. (2010). Comparison of linear voice coil and reluctance actuators for high-precision applications. In *Proceedings of 14th international power electronics and motion control conference EPE-PEMC 2010* (pp. S3–29 – S3–36). http://dx.doi.org/10.1109/EPEPEMC.2010.5606572.

Wang, Youqing, Gao, Furong, & Doyle, Francis J. (2009). Survey on iterative learning control, repetitive control, and run-to-run control. *Journal of Process Control*, *19*(10), 1589–1600. http://dx.doi.org/10.1016/j.jprocont.2009.09.006.

Xu, Jian-Xin (2011). A survey on iterative learning control for nonlinear systems. *International Journal of Control*, *84*(7), 1275–1294. http://dx.doi.org/10.1080/00207179.2011.574236.

Xu, Jian-Xin, & Tan, Ying (2003). Linear and nonlinear iterative learning control. *Lecture notes in control and information sciences*, Springer, http://dx.doi.org/10.1007/3-540-44845-4.

Xue, Xiangdang, Cheng, Ka Wai Eric, & Zhang, Zhu (2018). Model, analysis, and application of tubular linear switched reluctance actuator for linear compressors. *IEEE Transactions on Industrial Electronics*, *65*(12), 9863–9872. http://dx.doi.org/10.1109/TIE.2018.2818638.

Yang, Yee-Pien, Liu, Jieng-Jang, Ye, Da-Hau, Chen, Yi-Ruei, & Lu, Pai-Hsiu (2013). Multiobjective optimal design and soft landing control of an electromagnetic valve actuator for a camless engine. *IEEE/ASME Transactions on Mechatronics*, *18*(3), 963–972. http://dx.doi.org/10.1109/TMECH.2012.2195728.